Formation of a 10 Å phase with halloysite structure under hydrothermal conditions with varying initial chemical composition

Nikita A. Leonov[1,a], Daniil A. Kozlov[2,3,b], Demid A. Kirilenko[1,c], Nikolay A. Bert[1,d], Anna O. Pelageikina[1,e], Andrey A. Nechitailov[1,f], Mikhail B. Alikin[4,g], Andrei A. Krasilin[1,h]

[1]Ioffe Institute, St. Petersburg, Russia

[2]Lomonosov Moscow State University, Moscow, Russia

[3]Kurnakov Institute of General and Inorganic Chemistry, Russian Academy of Sciences, Moscow, Russia

[4]St. Petersburg State Technological University (Technical University), St. Petersburg, Russia

[a]nikita_leonov_1998@mail.ru, [b]danilko_zlov@mail.ru, [c]zumsisai@gmail.com, [d]ikolay.bert@mail.ioffe.ru, [e]Pelaanna@yandex.ru, [f]aan.shuv@mail.ioffe.ru, [g]alikinmix@gmail.com, [h]ikrasilin@mail.ioffe.ru

Corresponding author: N. A. Leonov, nikita_leonov_1998@mail.ru

ABSTRACT We studied the process of obtaining nanostructured halloysite by varying the parameters for creating the initial composition. The initial composition was synthesized by co-hydrolysis of $(C_3H_7O)_3Al$ and $(C_2H_5O)_4Si$ in the C_6H_{14}–$NH_3 \cdot H_2O$ system. Aluminum hydrosilicate with the composition $Al_2Si_2O_5(OH)_4$ was synthesized under hydrothermal conditions (220 °C, 2 MPa, 96 h). Particles of plate-like morphology with average length 100 – 200 nm and 60 nm thickness were obtained. The PXRD patterns revealed the presence of two phases. Plate-like kaolinites are found. Also we observed the formation of a halloysite-like phase. Studies of synthesized samples by IR spectroscopy and thermal analysis revealed the presence of organic-modified hydrosilicate with phase transition around 412 °C. The resulting phase is promising for studying the processes of adsorption and further exfoliation.

KEYWORDS aluminum, hydrosilicates, hydrothermal synthesis, kaolinite, halloysite

FOR CITATION Leonov N.A., Kozlov D.A., Kirilenko D.A., Bert N.A., Pelageikina A.O., Nechitailov A.A., Alikin M.B., Krasilin A.A. Formation of a 10 Å phase with halloysite structure under hydrothermal conditions with varying initial chemical composition. *Nanosystems: Phys. Chem. Math.*, 2023, **14** (2), 264–271.

1. Introduction

Recently, many works have been devoted to the use of layered hydrosilicates in various fields, including adsorption [1], catalysis [2] and the encapsulation of functional substances [3]. Hydrosilicates with the structure of imogolite [4], chrysotile [5,6] and halloysite [7] provided even more opportunities for such use due to their high specific surface area [8] and nanotubular morphology [9]. The latter originated from a number of structural peculiarities of the hydrosilicate layer, specifically, the size mismatch between metal-oxygen and silicon-oxygen sheets, as well as the difference in composition on the opposite sides of the layer [10]. Depending on structure type and chemical composition, scrolling can occur in various directions up to the formation of single-walled nanotubes [11] and sphere-like particles [12].

The functional properties of hydrosilicates may be enhanced by various methods of modification. Namely, metal-silicate composite materials were obtained from transition metal hydrosilicates by processing in hydrogen [13, 14], or in a solution containing a strong reducing agent under hydrothermal conditions [15], to produce magnetically controlled adsorbents and catalysts with a broad spectrum of activity. New metallic or oxide phases can also be imposed externally [16]. Some papers were devoted to the modification of the surface of hydrosilicates with acids [17, 18] and organic ligands [19–21].

Despite the wide range of applications for aluminum hydrosilicate nanoscrolls with halloysite structure, most researchers have been constrained to the use of the halloysite mineral. Attempts to synthesize nanoscrolls with halloysite structure by a hydrothermal process similar to one used to obtain chrysotile have not met with any significant success. According to the energy model of scrolling of hydrosilicate layers [22], these challenges arised due to the competition for scrolling direction fostered by the layer's tendency to minimize elastic and surface energies. It is noteworthy that this competition likely prevented the formation of not only aluminum hydrosilicate nanoscrolls with halloysite structure, but

also a whole range of structural analogs such as hydrogermanates of various metals [23]. To overcome these challenges, the following approaches are usually proposed:

(A) increasing size mismatch between the sheets by changing their chemical composition;
(B) changing the initial chemical composition structure;
(C) exfoliation of hydrosilicate layers with platy morphology.

In [24], the scrolling of aluminum hydrosilicate layers was observed only after a significant number of Si^{4+} ions were substituted for Ge^{4+}, which led to an increase in size mismatch between the sheets. At the same time, it is worth noting the results of [25], where the substitution of Si^{4+} for Ge^{4+} in nickel hydrosilicates with chrysotile structure resulted in the opposite effect, that is, the stabilization of plate-like morphology (see also [22]).

As far as we know, few papers have dealt with the application of approach B to the synthesis of nanotubular hydrosilicates with halloysite structure. In particular, work [26], which is available only in Russian, reported on the production of nanoscrolls with halloysite structure by hydrothermal treatment of a thermally pre-treated Al–Si-containing xerogel. A similar approach of using thermal annealing prior to hydrothermal treatment was used in [27]. These results, however, do not allow one to draw unequivocal conclusions in favor of the formation of nanoscrolls with halloysite structure. Finally, within the framework of approach C, hydrosilicate nanoscrolls can be obtained from plates using one [28] or several [29] stages of exfoliation, which indicates the key role of the interlayer interaction in stabilizing the plate-like morphology.

In this work, a further improvement of approach B to varying the initial chemical composition was proposed. It was shown in [22] that the main condition for the stabilization of plate-like morphology is a decrease in the specific surface energy on the edge surfaces of the hydrosilicate layer, which facilitates the thickening of model plates. The chemical reason for this phenomenon lies in the processes of surface hydroxylation, which is why attempts have been made to synthesize the initial compositions using anhydrous media.

2. Experimental

In total, 3 modes of synthesis of the initial composition were studied (Fig. 1): 1 – reverse precipitation of AlOOH from $AlCl_3 \cdot 6H_2O$ ("puriss.") with an aqueous solution of $NH_3 \cdot H_2O$ ("puriss. spec.") with amorphous SiO_2 (aerosil A-300, ("puriss.")); 2 – joint hydrolysis of $(C_3H_7O)_3Al$ ("X") and $(C_2H_5O)_4Si$ ("puriss.") in the C_6H_{14}–$NH_3 \cdot H_2O$ system; 3 – joint hydrolysis of the same compounds in the C_8H_{18}–$NH_3 \cdot H_2O$ system.
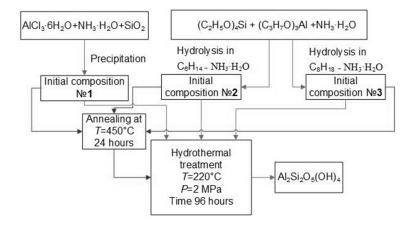

FIG. 1. Synthesis scheme

Synthesis mode 1 involved dispersing 3 g sample of SiO_2 in 27 ml of 2 M aqueous solution of $NH_3 \cdot H_2O$ with constant stirring for 1 hour. Next, 0.05 M aqueous solution of $AlCl_3$ was added drop by drop until the molar ratio of Al/Si = 1 was achieved. The resulting precipitate was washed with distilled water by centrifugation to a neutral reaction of the solution. Subsequently, the precipitate was dried in air at the temperature of 105 °C and ground in an agate mortar.

Synthesis mode 2 involved mixing 1.9 g sample of $(C_3H_7O)_3Al$ and 3.72 ml of $(C_2H_5O)_4Si$ in 90 ml of C_6H_{14} for 24 h. Next, 2 ml of 2 M aqueous solution of $NH_3 \cdot H_2O$ was added to the mixture and stirred for another 24 h. The resulting precipitate was washed with distilled water by centrifugation to a neutral reaction. After that, the precipitate was dried in air at the temperature of 80 °C and ground in an agate mortar. The molar excess $(C_2H_5O)_4Si$ was pre-established experimentally by energy-dispersive X-ray spectroscopy (EDS) of the Al/Si ratio in the initial composition (Fig. 2). Analogical procedures were followed for synthesis mode 3, which used the C_8H_{18} homologue with a longer chain to synthesize the initial composition.

Prior to hydrothermal treatment, parts of the dried and ground sediments of the initial compositions with masses of 2 g were pre-annealed in air at 450 °C at a heating rate of 5 °/min. The isothermal holding time was 24 h with cooling in the furnace (Fig. 1). The samples of the initial compositions and annealing products weighting 0.2 g underwent
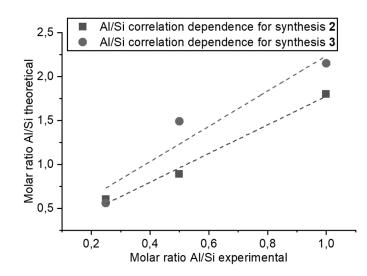
FIG. 2. Correlation dependence of Al/Si for hydrolysis in mixtures C_6H_{14}–$NH_3 \cdot H_2O$ and C_8H_{18}–$NH_3 \cdot H_2O$

hydrothermal treatment in PTFE-lined autoclaves with a capacity of 25 ml at a temperature of 220 °C and pressure of 2 MPa for 96 h. Distilled water was used as a hydrothermal medium. The products of hydrothermal treatment were dried in air at a temperature of 80 °C.

The phase composition of the products of hydrothermal treatment and thermal annealing was studied by powder X-ray diffraction (PXRD) using a Rigaku SmartLab 3 diffractometer (CuKα-radiation). The analysis of the obtained X-ray diffractograms was carried out using the ICDD PDF-2 database. The morphology of the products of hydrothermal treatment and thermal annealing, as well as elemental analysis, were studied on a FEI Quanta 200 scanning electron microscope (SEM) with an integrated EDAX X-ray Si(Li) spectrometer. In addition, the morphology of hydrothermal treatment and thermal annealing was studied using a transmission electron microscope (TEM) JEM-2100F and Tescan Amber GMH in scanning transmission electron microscopy (STEM) mode. Synchronous thermal analysis was performed on a Mettler Toledo TGA/DSC 1-Star system in the 35 – 992 °C temperature range. IR spectra were taken with a Shimadzu IRTracer-100 Fourier transform-infrared spectrometer at room temperature (Shimadzu, Kyoto, Japan). The spectra were recorded by averaging of 64 scans in the range from 4000 to 350 cm^{-1} with a resolution of 4 cm^{-1} in KBr tablets.

3. Results and discussion

The PXRD patterns of the hydrothermal treatment (HTT) products of synthesis variants 1, 2 and 3 before and after annealing at 450 °C are shown in Fig. 3. The main phase formed during HTT is plate-like kaolinite $Al_2Si_2O_5(OH)_4$. The only exception is the sample obtained during the HTT of the initial composition synthesized in mode 2 (without pre-annealing). In this case, the formation of a phase with extended period (up to 10 Å) was observed, which was similar to the 10 Å phase of halloysite $Al_2Si_2O_5(OH)_4 \cdot 2H_2O$. Preliminary thermal annealing of the initial compositions at 450 °C and HTT resulted in either a decrease in the intensity of the main kaolinite reflexes (in the case of synthesis variants 1 and 3) and the formation of an amorphous phase, or the disappearance of the 10 Å phase from the products of HTT (in the case of synthesis 2).

The electron microscopy study of the HTT products showed (Figs. 4 and 5) that the particles had plate-like morphology regardless of whether the initial compositions were pre-annealed or not. The length of the plates was 50 – 200 nm, while the thickness varied from 10 up to 60 nm.

The analysis of the elemental composition (Table 1) showed that the content of possible impurities was below the detection limit in all samples, and the molar Al/Si ratio was either close to stoichiometric for the halloysite formula of $Al_2Si_2O_5(OH)_4$.

Figures 6 and 7 show the IR spectra of the studied samples. According to [30, 31], the absorption bands in the region of 1640 – 1650 cm^{-1} were caused by the deformation vibrations of H–O–H water molecules in the interlayer space and the physically sorbed water. The absorption band at 916 cm^{-1} is related to the Al–OH. The bands at 796 and 755 cm^{-1} corresponded to Si–O–Al bond vibrations. In the same region, Si–O valence vibrations were also manifested. Intense bands of 1000 – 1050 cm^{-1} and 696 with complex contouring were caused by in-plane stretching vibrations and sharp stretching vibration. The bands at 544 and 467 cm^{-1} correspond to the in-plane stretching vibrations of the Si–O–Al and Si–O–Si groups.

Let us consider in more details the part of the IR spectrum in the region of valence vibrations of hydroxyl groups (3300 – 3800 cm^{-1}). The complex character of the bands in the region of O–H valence vibrations was due to the different environments in which these groups are located, as well as the presence of impurity phases, for example, gibbsite (see
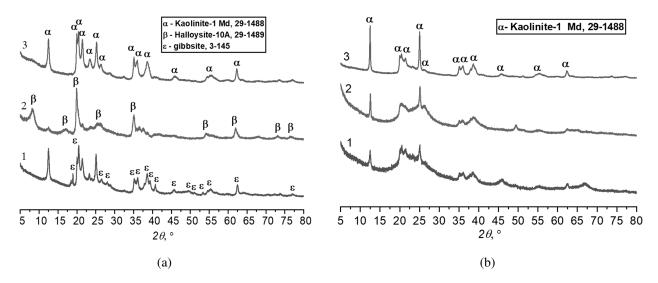
FIG. 3. X-ray diffraction patterns of the products of hydrothermal treatment of 1, 2 and 3 modes of synthesis before thermal annealing of the initial composition (a) and after annealing of the initial composition at 450 °C (b)
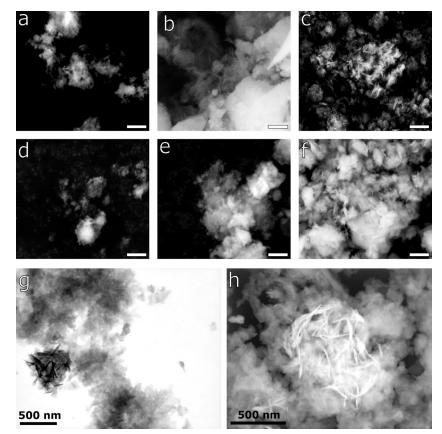

FIG. 4. SEM (a–f) and STEM (g–h) micrographs of hydrothermal treatment products: a, b, c – 1, 2 and 3 modes of synthesis; d, e, f – 1, 2 and 3 modes of synthesis after annealing of the initial composition at 450 °C (scale bar 2 μm); g,h – hydrothermal treatment product of mode 2
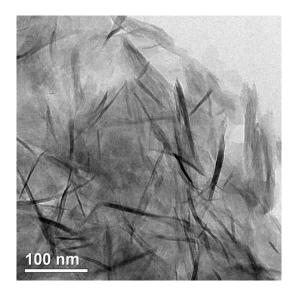
FIG. 5. TEM micrograph of the hydrothermal treatment product of synthesis mode 2

TABLE 1. Elemental composition of the HTT products of the initial compositions before and after pre-annealing at 450 °C (according to EDS)

Initial composition	Elemental composition, at. %			Al/Si
	O	Al	Si	
1	63.4±0.7	18.2±0.2	18.4±0.5	0.99±0.01
2	62.9±6.1	16.5±2.6	20.6±3.6	0.80±0.04
3	63.9±1.3	17.4±0.7	18.7±0.9	0.93±0.05
1 (450 °C)	63.2±3.1	17.4±7.8	19.4±4.8	0.9±0.6
2 (450 °C)	65.2±1.8	17.4±1.6	17.3±0.4	1.02±0.08
3 (450 °C)	61.5±0.8	17.9±0.2	20.6±0.7	0.87±0.02

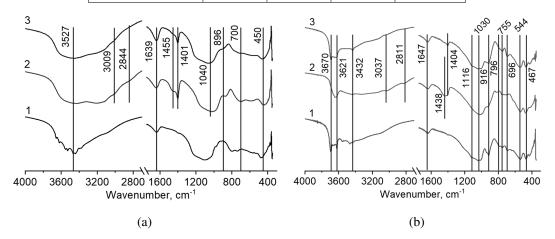(a)   (b)

FIG. 6. IR transmission spectra of initial compositions (a) and products of hydrothermal treatment (b) of 1, 2 and 3 modes of synthesis
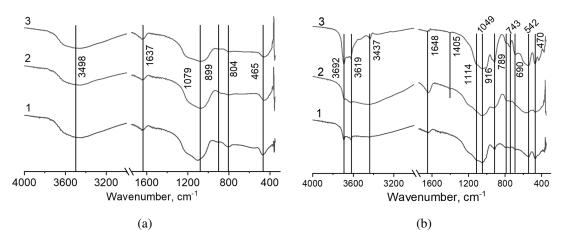
FIG. 7. IR transmission spectra of the initial compositions after annealing at 450 °C (a), as well as the products of their hydrothermal treatment (b) of 1, 2 and 3 modes of synthesis

Fig. 3). In accordance with the structure of halloysite and kaolinite [32], hydroxyl groups were divided into "inner surface" O–H and "inner" O–H. The interlayer (inner O–H) groups are located between silicon oxide tetrahedra and aluminum oxide octahedra. The inner surface O–H groups are located in the interlayer space and are connected only to aluminum oxide octahedra [32]. The band at 3670 cm^{-1} corresponded to the valence vibrations of OH groups on the surface of the inner layer of the nanotube, whereas the band at 3621 cm^{-1} corresponded to the valence vibrations of the interlayer OH groups. Additionally, the adsorbed water manifested itself in the form of a wide band in the region of 3500 cm^{-1}.

The bands at 3037, 2811 and 1405 cm^{-1} correspond to symmetric, asymmetric and scissor-like valence vibrations of stretching and deformation of CH$_2$ [33], which indicate the presence of an organic component in the system. There is also a band at 1438 cm^{-1} in the spectrum presumably corresponding to the vibration of C–O–Al bonds. HTT leaded to a significant decrease in the intensity of these bands but did not completely remove them. In contrast, preliminary thermal annealing at 450 °C leaded to the disappearance of all bands associated with organic groups (Fig. 7).

Figure 8 illustrates the results of synchronous thermal analysis of the initial composition synthesized in mode 2 and the product of its HTT. The initial composition was characterized by a continuous loss of mass throughout the studied temperature range. According to IR spectroscopy data (Fig. 6), mass losses at the initial stage were associated with the removal of adsorbed water [34], as well as the removal of organic compounds. In a higher temperature region, the differential curve showed an effect associated with volumetric dehydroxylation of the hydrosilicate phase [35–37] in the initial composition. Following the hydrothermal treatment, the mass loss of the sample was significantly reduced (and practically absent in the range of 120 – 300 °C), which indicated a likely decrease in the specific surface area as a result of recrystallization and fewer opportunities for adsorption of water or organic solvent. The first thermal effect and the associated mass loss following HTT were observed at a relatively low temperature (below 100 °C), which correlated with the temperature of removal of interlayer water molecules from the structure of 10 Å halloysite [38]. With an increase in temperature, a series of effects were distinctly observed on the DTG curve that are also associated with volumetric dehydroxylation of hydrosilicates. However, unlike in the case of the original composition, there are several stages of mass loss. The highest high-temperature peak (528 °C) corresponds to the transformation of the 7 Å impurity phase (Fig. 3(a)), while the average peak in the series (480 °C) correlates to the greatest extent with the literature data on 10 Å halloysite [38]. The origin of the first peak of the series (412 °C) may be associated with the transition of the organically modified part of the hydrosilicate.

4. Conclusion

Layered aluminum hydrosilicates were obtained by hydrothermal treatment of initial compositions with various chemical prehistory. The formation of a 10 Å phase with a 10 Å halloysite structure was observed when using Al(OC$_3$H$_7$)$_3$ and Si(OC$_2$H$_5$)$_4$ as the initial reagents of the product of the alkaline co-hydrolysis in the C$_6$H$_{14}$–NH$_3$·H$_2$O system. The increased distance between the hydrosilicate layers was created by organic ligands as evidenced by IR spectroscopy data. The use of traditional precipitation, annealing of initial compositions before the hydrothermal treatment, as well as varying the length of the organic solvent molecule led to the formation of a 7 Å phase with kaolinite structure. Although the increase in the interlayer distance was not enough to overcome the trend of the interlayer interaction and the formation of nanoscrolls, the resulting phase is promising for studying the processes of adsorption and further exfoliation.
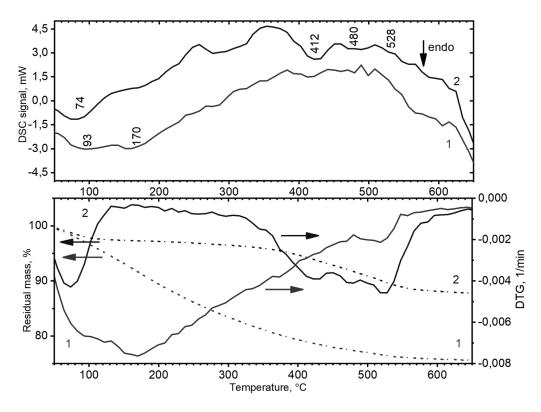
FIG. 8. DSC curves of thermal effects, thermogravimetry curves obtained in a dynamic air atmosphere for the initial composition (1) and the product of hydrothermal treatment of synthesis mode 2 (2)

References

[1] Pimneva L.A. Study of the adsorption of manganese ions (II) in natural kaolinite. *Modern high technologies*, 2017, **7**, P. 61–65.

[2] Minyukova T.P., Shtertser N.V., Khassin A.A., Plyasova L.M., Kustova G.N., Zaikovskii V.I., Baronskaya N.A., Kuznetsova A.V., Davydova L.P., Yur'eva T.M., Shvedenkov Yu.G., Van Den Heuvel J.C. Evolution of Cu–Zn–Si oxide catalysts in the course of reduction and reoxidation as studied by in situ x-ray diffraction analysis, transmission electron microscopy, and magnetic susceptibility methods. *Kinetics and Catalysis*, 2008, **49** (6), P. 821–830.

[3] Bikbau M.Ya. Nano cement morphological peculiarities, structure properties and concrete on their base. *Concrete technology*, 2014, **4**, P. 38–44.

[4] Koji Wada, Naganori Yoshinaga. The structure of "imogolite". *American Mineralogist*, 1969, **52** (1–2), P. 50–71.

[5] Levin A., Khrapova E., Kozlov D., Krasilin A., Gusarov V. Structure refinement, microstrains and crystallite sizes of Mg–Ni-phyllosilicate nano-scroll powders. *J. Appl. Cryst.*, 2022, **55**, P. 484–502.

[6] Bates T.F., Sand L.B., Mink J.F. Tubular Crystals of Chrysotile Asbestos. *Science*, 1950, **111**, P. 512–513.

[7] Bates T.F., Hildebrand F.A., Swineford A. Morphology and structure of endellite and halloysite. *American Mineralogist*, 1950, **35** (7–8), P. 463–484.

[8] Lukuttsova N.P., Golovin S.N. Aggregative stability of aqueous suspensions of halloysite nanotubes. *Construction materials*, 2018, **1** (2), P. 4–10.

[9] Arsent'ev M.Y., Golubeva O.Y. Comparative Study of Internal Mechanical Stresses in the Structures of Montmorillonite and Halloysite. *Glass Phys. Chem.*, 2020, **46**, P. 598–604.

[10] Szczepanik B., Slomkiewicz P., Garnuszek M., Czech K., Banas D., Kubala-Kukus A., Stabrawa I. The effect of chemical modification on the physico-chemical characteristics of halloysite: FTIR, XRF, and XRD studies. *J. of Molecular Structure*, 2015, **1084**, P. 16–22.

[11] Krasilin A.A., Khrapova E.K., Maslennikova T.P. Cation Doping Approach for Nanotubular Hydrosilicates Curvature Control and Related Applications. *Crystals*, 2020, **10**, 654.

[12] Parfitt R.L., Furkert R. J., Henmi T. Identification and Structure of Two Types of Allophane from Volcanic Ash Soils and Tephra. *Clays and Clay Minerals*, 1980, **28**, P. 328–334.

[13] Krasilin A.A., Khrapova E.K., Nominé A., Ghanbaja J., Belmonte T., Gusarov V.V. Cation Redistribution along the Spiral of Ni-Doped Phyllosilicate Nanoscrolls: Energy Modelling and STEM/EDS Study. *Chem. Phys. Chem.*, 2019, **20**, P. 1–9.

[14] Kirichenko O.A., Shuvalova E.V., Redina, E.A. Low-temperature copper hydrosilicates: catalysts for reduction of aromatic nitro compounds with molecular hydrogen. *Russ. Chem. Bull.*, 2019, **68**, P. 2048–2052.

[15] Hara T., Mascotto S., Weidmann C., Smarsly B.M. The effect of hydrothermal treatment on column performance for monolithic silica capillary columns. *J. of Chromatography A*, 2011, **1218**, P. 3624–3635.

[16] Krasilin A.A., Bodalyov I.S., Malkov A.A., Khrapova E.K., Maslennikova T.P., Malygin A.A. On an adsorption/photocatalytic performance of nanotubular $Mg_3Si_2O_5(OH)_4/TiO_2$ composite. *Nanosystems: Phys. Chem. Math.*, 2018, **9** (3), P. 410–416.

[17] Krasilin A.A., Straumal E.A., Yurkova L.L., Khrapova E.K., Tomkovich M.V., Shunina I.G., Vasil'eva L.P., Lermontov S.A., Ivanov V.K. Sulfated Halloysite Nanoscrolls as Superacid Catalysts for Oligomerization of Hexene-1. *Russ. J. Appl. Chem.*, 2019, **92**, P. 1251–1257.

[18] Sidorenko A.Yu., Kravtsova A.V., Aho A., Heinmaa I., Wärna J., Pazniak H., Volcho K.P., Salakhutdinov N.F., Murzin D.Yu., Agabekov V.E. Highly selective Prins reaction over acid-modified halloysite nanotubes for synthesis of isopulegol-derived 2H-chromene compounds. *J. of Catalysis*, 2019, **374**, P. 360–377.

[19] Thill A., Picot P., Bellon L. A mechanism for the sphere/tube shape transition of nanoparticles with an imogolite local structure (imogolite and allophane). *Applied Clay Science*, 2017, **141**, P. 308–315.

[20] Pigniè M.-C., Shcherbakov V., Charpentier T., Moskura M., Carteret C., Denisov S., Mostafavi M., Thill A., Caër S. Confined water radiolysis in aluminosilicate nanotubes: the importance of charge separation effects. *Nanoscale*, 2021, **13**, P. 3092–3105.

[21] Cavallaro G., Lazzara G., Milioto S., Parisi F., Sanzillo V. Modified Halloysite Nanotubes: Nanoarchitectures for Enhancing the Capture of Oils from Vapor and Liquid Phases. *ACS Appl. Mater. Interfaces*, 2014, **6**, P. 606–612.

[22] Krasilin A.A. Energy modeling of competition between tubular and platy morphologies of chrysotile and halloysite layers. *Clays and Clay Minerals*, 2020, **1**, P. 1–12.

[23] Krasilin A.A., Khrapova E.K. Effect of hydrothermal treatment conditions on formation of nickel hydrogermanate with platy morphology. *Russ. J. Appl. Chem.*, 2017, **90**, P. 22–27.

[24] White R.D., Bavykin D.V., Walsh F.C. Spontaneous Scrolling of Kaolinite Nanosheets into Halloysite Nanotubes in an Aqueous Suspension in the Presence of GeO_2. *J. of Physical Chemistry*, 2012, **116**, P. 8824–8833.

[25] Perbost R., Amouric M., Olives J. Influence of Cation Size on the Curvature of Serpentine Minerals: HRTEM-AEM Study and Elastic Theory. *Clays Clay Miner.*, 2003, **51**, P. 430–438.

[26] Maslennikova T.P., Korytkova E.N., Pivovarova L.N. Hydrothermal synthesis of nanotube composition $Al_2Si_2O_5(OH)_4 \cdot 2H_2O$ with halloysite structure. *Physics and Chemistry of Glass*, 2012, **S6**, P. 890–893.

[27] Golubeva O.Yu, Alikina Y.A., Kalashnikova T.A. Influence of hydrothermal synthesis conditions on the morphology and sorption properties of porous aluminosilicates with kaolinite and halloysite structures. *Applied Clay Science*, 2020, **199**, P. 1–12.

[28] Makóa É., Kovács A., Antal V., Kristóf T. Thin-walled nanoscrolls by multi-step intercalation from tubular halloysite-10 Å and its rearrangement upon peroxide treatment. *Applied Clay Science*, 2017, **146**, P. 131–139.

[29] Xiaoguang Li, Qinfu Liu, Hongfei Cheng, Sridhar Komarneni. High-yield production of mesoporous nanoscrolls from kaolinite by ultrasonic assisted exfoliation. *Microporous and Mesoporous Materials*, 2017, **241**, P. 66–71.

[30] Kloprogge J.T. Characterisation of Halloysite by Spectroscopy. *Developm. Clay Sci.*, 2016, **7**, P. 115–136.

[31] Jiangyan Yuan, Jing Yang, Hongwen Ma, Shuangqing Su, Qianqian Chang, Sridhar Komarneni. Hydrothermal synthesis of nano-kaolinite from K-feldspar. *Ceramics International*, 2018, **44** (13), P. 15611–15617.

[32] Tan D., Yuan P., Liu D., Du P. Chapter 8 - Surface Modifications of Halloysite. *Developm. Clay Sci.*, 2016, **7**, P. 167–201.

[33] Weng On Yah, Atsushi Takahara, Yuri M. Lvov. Selective Modification of Halloysite Lumen with Octadecylphosphonic Acid: New Inorganic Tubular Micelle. *J. of the American Chemical Society*, 2012, **134** (3), P. 1853–1859.

[34] Li Y., Zhang Y., Zhang Y., Liu M., Zhang F., Wang L. Thermal behavior analysis of halloysite selected from Inner Mongolia Autonomous Region in China. *J. Therm. Anal. Calorim.*, 2017, **129**, P. 1333–1339.

[35] Erzsébet Horváth, Ray L. Frost, Éva Makó, János Kristóf, Tamás Cseh. Thermal treatment of mechanochemically activated kaolinite. *Thermochimica Acta*, 2003, **404** (1–2), P. 227–234.

[36] Gábor M., Tóth M., Kristóf J., Komáromi-Hiller G. Thermal Behavior and Decomposition of Intercalated Kaolinite. *Clays Clay Miner.*, 1995, **43**, P. 223–228.

[37] Krasilin A.A., Danilovich D.P., Yudina E.B., Bruyere S., Ghanbaja J., Ivanov V.K. Crystal violet adsorption by oppositely twisted heat-treated halloysite and pecoraite nanoscrolls. *Applied Clay Science*, 2019, **173**, P. 1–11.

[38] Joussein E., Petit S., Churchman J., Theng B., Righi D., Delvaux B. Halloysite clay minerals – a review. *Clay Minerals*, 2005, **40**, P. 383–426.

Information about the authors:

Nikita A. Leonov – Ioffe Institute, 26 Politekhnicheskaya, 194021, St. Petersburg, Russia; ORCID 0000-0001-8886-0731; nikita_leonov_1998@mail.ru

Daniil A. Kozlov – Lomonosov Moscow State University, Leninsky gory, 1, 119991, Moscow, Russia; Kurnakov Institute of General and Inorganic Chemistry, Russian Academy of Sciences, Leninsky pr., 31, 119991, Moscow, Russia; ORCID 0000-0003-0620-8016; kozlov@inorg.chem.msu.ru

Demid A. Kirilenko – Ioffe Institute, 26 Politekhnicheskaya, 194021, St. Petersburg, Russia; ORCID 0000-0002-1571-209X; zumsisai@gmail.com

Nikolay A. Bert – Ioffe Institute, 26 Politekhnicheskaya, 194021, St. Petersburg, Russia; ORCID 0000-0001-6136-4877; nikolay.bert@mail.ioffe.ru

Anna O. Pelageikina – Ioffe Institute, 26 Politekhnicheskaya, 194021, St. Petersburg, Russia; ORCID 0009-0000-6320-2011; Pelaanna@yandex.ru

Andrey A. Nechitailov – Ioffe Institute, 26 Politekhnicheskaya, 194021, St. Petersburg, Russia; ORCID 0000-0002-9895-6822; aan.shuv@mail.ioffe.ru

Mikhail B. Alikin – St. Petersburg State Technological University (Technical University), 190013, St. Petersburg, Russia; ORCID 0000-0002-0770-9675; alikinmix@gmail.com

Andrei A. Krasilin – Ioffe Institute, 26 Politekhnicheskaya, 194021, St. Petersburg, Russia; ORCID 0000-0002-3938-3024; ikrasilin@mail.ioffe.ru

Conflict of interest: the authors declare no conflict of interest.